Biophysical Chemistry 18 (1983) 381–390
Elsevier

BPC 00817

DIELECTRIC BEHAVIOR OF POLYELECTROLYTES

III. THE ROLE OF COUNTERION INTERACTIONS

Gary E. WESENBERG and Worth E. VAUGHAN

Department of Chemistry, University of Wisconsin-Madison, Madison, WI 53706, U.S.A.

Received 27th April 1983
Revised manuscript received 26th July 1983
Accepted 2nd August 1983

Key words: Polyelectrolyte; Dielectric response; Counterion interaction

The role of the Coulomb forces between the counterions on the surface of polyelectrolytes on the dielectric response is analyzed. An estimate of the maximum dielectric increment (as a function of the number of counterions) is found as a function of the molecular length. The minimum-energy configuration of the counterions on a cylinder is found to be a double helix, suggesting the fundamental importance of electrostatic interactions in determining structure. Solutions of the dynamical equations for a few counterions indicate that a single mode dominates the relaxation which is enhanced by the inter-ion repulsions. A lower bound is found for this mode based on analysis of the system response for short lengths. Sum rules for the rates and amplitudes of the dipolar correlation function are derived and lead to an upper bound for the rate of the dominant mode. These bounds approach one another for the parameters characteristic of restriction fragments of DNA. This permits a prediction of the magnitude and time scale of the dielectric response.

1. Introduction

In previous work (papers I [1] and II [2] of this series), the dipolar correlation function γ of a cylindrical (or linear) model polyelectrolyte was found from the solution of the coupled forced diffusion of the counterions in bulk and on the polyelectrolyte

$$\gamma = \langle \mu(t) \cdot \mu(0) \rangle \tag{1}$$

where the average is taken over the equilibrium distribution and μ is the dipole moment of the system

$$P_{eq} = \exp(-V/k_B T)/\Sigma \int_0^L \exp(-V/k_B T)\mathrm{d}\tau \tag{2}$$

$$V = \sum_{j<i} \sum_i e^2/4\pi\epsilon\epsilon_0 |r_i - r_j|. \tag{3}$$

The potential function describing the counterion interactions entered the calculation in two places.

V appears explicitly in eq. 1 via eqs. 2 and 3. This interaction determines the magnitude of the dielectric increment as reflected in $\gamma(0)$. Although our previous calculations suggested a maximum in the dielectric increment as a function of the number, n', of counterions, the value and location of the maximum were very uncertain for many particle systems (such as DNA).

Here we examine in more detail the dependence of the dielectric increment on the number of counterions constrained to the polyelectrolyte surface and on the length of the polyelectrolyte molecule. A simple relation involving the maximum dielectric increment is found that allows convincing extrapolation to systems with large numbers of counterions.

The potential V also appears in the forcing

terms in the diffusion equation chosen to model the system dynamics. Previously, we argued [1] that the potential could be replaced by its Taylor series expansion (through quadratic terms) about the most probable distribution. The rationale for this step was that only system configurations in the vicinity of the most probable distribution would escape annihilation by the integration over P_{eq}. The effect of this approximation was to subtract a constant from the rates of all relaxation modes. Estimates of the constant indicated that it was large, but no evaluation of the range of applicability of the truncated Taylor series approximation was performed. Here we attack the role of the potential on the dynamics head-on and find that the potential plays a major role and enhances the relaxation rate.

2. Static properties

2.1. The dielectric increment

For simplicity we restrict discussion to the linear case [1]. The method is the same for more complicated (cylindrical) geometries [2]. Eq. 3 becomes

$$V/k_BT = \sum_{j<1}\sum_{i} e^2/4\pi\epsilon\epsilon_0 k_BT(z_i - z_j) = \sum_{j<i}\sum_{i} B/(x_i - x_j) \tag{4}$$

where the range of z_i is 0 to L and the range of x_i is -1 to 1. The linear array of ions is such that $x_i > x_j$. Clearly, B is proportional to $1/L$. Taking $L = 51$ nm as a typical length for a segment of DNA, in water at 300 K $B = 0.028$.

The system dipole moment is

$$\mu = e\sum_i (z_i - L/2) = eL\sum x_i/2 \tag{5}$$

In units of $e^2L^2/4$ eq. 1 becomes

$$\gamma(0) = c\int_{-1}^{1}\int_{-1}^{1}\left[\sum x_i\right]^2 \exp(-V/k_BT)\prod_i dx_i \tag{6}$$

where

$$1/c = \int_{-1}^{1}\int_{-1}^{1}\exp(-V/k_BT)\prod_i dx_i. \tag{7}$$

We seek the dependence of $\gamma(0)$ on n' and L. For $n' = 1$ and $n' = 2$ the integrals in eqs. 6 and 7 were evaluated by Romberg quadrature. For $n' > 2$,

Table 1

Values of $\gamma(0)$

System parameters are $L = 51$ nm, $T = 300$ K. The model used is indicated in the first column. Standard errors are shown for large n'.

n'	B							
	0.001	0.010	0.028	0.100	0.500	1.000	5.000	10.000
1(A)	0.330	0.313	0.294	0.249	0.158	0.115	0.039	0.022
1(B)	0.333	0.333	0.333	0.333	0.333	0.333	0.333	0.333
2(A)	0.656	0.608	0.550	0.430	0.228	0.150	0.042	0.022
2(B)	0.663	0.645	0.621	0.563	0.422	0.337	0.134	0.070
3(A)	0.981	0.884	0.775	0.563	0.258	0.159	0.040	0.021
3(B)	0.988	0.935	0.870	0.723	0.428	0.291	0.075	0.035
5(A)	1.616	1.385	1.146	0.736	0.274	0.156	0.036	0.019
5(B)	1.630	1.464	1.276	0.909	0.382	0.220	–	–
10(A)	3.145	2.399	1.752	0.899	–	–	–	–
10(B)	3.175	2.524	1.920	1.037	–	–	–	–
15(A)	–	–	2.096 (0.01)	–	–	–	–	–
20(A)	–	–	2.31 (0.04)	–	–	–	–	–
20(B)	–	–	2.58	–	–	–	–	–
25(A)	–	–	2.55 (0.07)	–	–	–	–	–
30(A)	–	–	2.46 (0.26)	–	–	–	–	–
30(B)	–	–	2.94	–	–	–	–	–
35(A)	–	–	2.73 (0.55)	–	–	–	–	–
40(A)	–	–	3.41 (1.39)	–	–	–	–	–
40(B)	–	–	2.94	–	–	–	–	–

Monte-Carlo integration was employed.

In order to examine the role of end effects two different models were used. In one model (A) two (additional) ions were fixed at the end points. In the other model (B) no fixed charges were imposed on the systems.

The results of the calculation are shown in table 1.

As n' increases for fixed B, $\gamma(0)$ rises rapidly to a plateau value and then declines slowly. The effect is most easily seen in the data for B around 0.5. For large B the rising portion is not well defined as it occurs for very small n' whereas for small B the plateau value is not reached before errors in the Monte-Carlo integrations degrade the data.

Some of the data are plotted in fig. 1. The solid line is the independent particle prediction $\gamma(0) = n'/3$ (units $e^2L^2/4$). Even for moderate B (0.028) and small n' the onset of saturation is evident. The points for model A lie below those for model B, reflecting the additional repulsions due to the particles fixed at the end points. This is an end effect which washes out for larger n'.

The dotted line is a prediction for the maximum in $\gamma(0)$ when $B = 0.028$. For the series of B in the range $0.1 < B < 2.0$ accurate estimates of the plateau value are found. If the logarithm of the plateau values is plotted versus the logarithm of B, an approximate straight line develops (fig. 2) which permits extrapolation out of the region (range of B) for which the plateau value is well established. The extrapolation to $B = 0.028$ is shown by the dotted line in fig. 2. The resulting $\gamma(0)$ for $B = 0.028$ is shown in fig. 1. Clearly, this estimate is compatible with the direct Monte-Carlo evaluations.

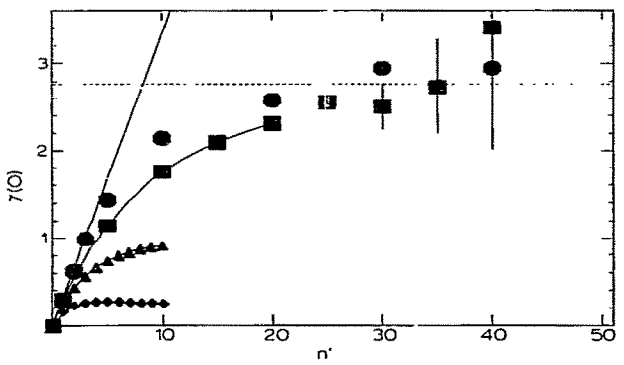

Fig. 1. Amplitude of the correlation function. Squares (model A). Circles (model B). (Solid line) The independent particle prediction. (Dotted line) Extrapolation to $B = 0.028$. (Triangles) $B = 0.1$. (Diamonds) $B = 0.5$. The curved lines are cubic splines through the data.

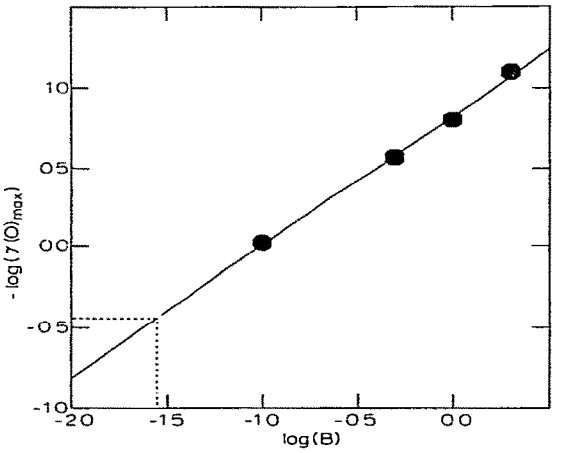

Fig. 2. The plateau value of the correlation function amplitude as a function of the strength of the counterion interaction. (Solid line) Linear fit. (Dotted lines) Extrapolation to $B = 0.028$.

2.2. *The configuration of minimum energy*

A viable approach to the evaluation of the integrals of eqs. 6 and 7 is to expand the integrands in Taylor series about the configuration of minimum energy. The resulting series can be integrated term by term and the bookkeeping can be done by computer.

As a preliminary step in this direction we have evaluated the configurations of minimum energy for linear and cylindrical arrays of n' counterions. For this calculation no auxiliary charge distribution is assigned.

For linear arrays the particles appear symmetrically about the midpoint with a tendency to bunch towards the ends where repulsive interactions are less. The case of cylindrical geometry is more interesting. In parallel with results found for

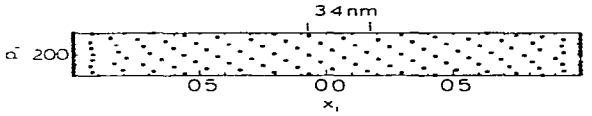

Fig. 3. Cartesian representation of the equilibrium configuration of 114 particles on a cylinder of length $L = 25.5$ nm and radius $r = 1.3$ nm. Particles with $\phi < 40°$ are plotted twice as the y-axis spans $0 \leq \phi \leq 400°$. The distance between the vertical lines is 3.4 nm.

spherical constraints [3] a variety of distinct shapes emerge. For $n' = 10$, as the ratio of cylinder radius to length decreases, one passes from eclipsed pentagons on the cylinder ends, to distorted squares on each end with a dumbbell in the center, to a configuration similar to that corresponding to the linear array.

To model a representative fragment of DNA we chose $L = 25.5$ nm, $n' = 114$ and a radius of 1.3 nm. The minimum energy configuration in the ϕ-x plane (with an overlapping portion of ϕ space) is shown in fig. 3. A stereographic projection is shown in fig. 4.

The central portion of the array has the form of a double helix. Further, the pitch of the helix is 3.3 nm per turn which compares with 3.4 nm per turn for the phosphate backbone in DNA. These results suggest a significant electrostatic component in determining the structure of DNA. If the phosphate charges are modeled by a uniform linear distribution of charge along the cylinder axis, the positive charges are drawn in from the ends but the central portion is not affected significantly. A uniform potential added to eq. 4 shows up only as an end effect. We are presently investigating the range of cylinder geometries and values of n' for which the helical configuration persists.

The configuration of minimum energy is not easily found (for cylindrical arrays) by direct minimization of eq. 3 as the minimum occurs (in part) with coordinates at the boundary of configuration

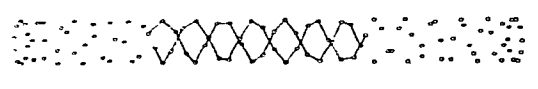

Fig. 4. Stereographic projection of the data shown in fig. 3. The points in the mid-region are connected by straight lines.

space. Rather, the system dynamics were described by the Langevin equation (see appendix B), the inertial and random force terms discarded, and the system equations of change solved by Runge-Kutta integration. The asymptotic system final state was reached after roughly 10000 iterations and appears to be independent of the initial configuration. Details are shown in ref. 4.

3. The role of V in the dynamics

To focus on the role of the forcing terms due to the potential in the system dynamics we specialize to the linear case and omit terms associated with the dissociation and reassociation of counterions on the polyelectrolyte surface (see refs. 1 and 2 for the complete formalism).

The model diffusion equation is then given by

$$\frac{\partial P}{\partial t} = D_1 \sum_i \frac{\partial^2 P}{\partial z_i^2} + \frac{D_1}{k_B T}\left[\sum_i P \frac{\partial^2 V}{\partial z_i^2} + \sum_i \frac{\partial V}{\partial z_i}\frac{\partial P}{\partial z_i}\right] \tag{8}$$

where V is given by eq. 3, D_1 is the one-dimensional diffusion constant, the sum is over the counterions, and P (system Green function) is the conditional probability density of finding the system with a configuration $\{z_i\}$ at time t given a configuration $\{z_i'\}$ at $t = 0$. Evaluation of the dipolar correlation function involves integration over both sets of coordinates.

$$\gamma = e^2 \int_0^L \int_0^L \prod_i \mathrm{d}z_i' \sum_i \left(z_i' - \frac{L}{2}\right) P_{\mathrm{eq}} \int_0^L \int_0^L \prod_i \mathrm{d}z_i \sum_i \left(z_i - \frac{L}{2}\right) P \tag{9}$$

The form of eq. 8 ensures that γ has the form

$$\gamma = \sum_j c_j \exp(-\lambda_j t). \tag{10}$$

We find (below) that the smallest λ_j (λ_1) is associated with the largest C_j and thus we will pay particular attention to the estimation of λ_1. This dominance of the relaxation function by its slowest term appears to be a widespread phenomenon. It appears in the mechanical relaxation of polymers with excluded volume (for example, see ref. 5).

Solutions to eq. 8 do not come easily for $n' = 1$, much less for larger n'. Fourier expansion or trans-

formation produced divergent integrals involving the derivatives of V. Expansion of V and the spatial part of the solution in power series did not yield a closed-form equation nor a numerically applicable expression for the λ_j. Thus, numerical methods were employed from the outset.

We are interested in the moderate B large n' regime. For example, our typical DNA fragment has $n' = 228$ and $B = 0.028$. The dynamics can be solved for small n' and large B. To connect these two cases appears hopeless. However, we succeed (below) in mapping one regime onto the other. In fact, from the standpoint of the forces felt by the individual ions, the regimes are comparable. With large n' the particles are forced together and a modest B causes a large force. If B is large, the force will be large even though only a few particles are present. Thus, we start by analysis of the cases $n' = 1$ and $n' = 2$.

The spatial derivatives in eq. 8 may be replaced by divided differences, the grid size being taken sufficiently large so that the results are independent of grid size [6]. Eq. 8 then turns into a set of coupled linear first-order differential equations which may be solved in principle by standard methods [4]. This approach, leading to $\{c_i, \lambda_i\}$, was implemented for $n' = 1$. Results (model A) are shown in table 2.

The first mode (smallest λ) dominates the relaxation behavior as indicated by the fraction of the total amplitude, c_1', associated with the first mode. The next mode is well separated (see the result for $B = 1.00$) and carries essentially all of the remaining amplitude. Thus, for $n' = 1$ at least one may approximate γ by a simple exponential.

Table 2

Relaxation parameters ($n' = 1$)

B	λ_1	C_1'
0.028	2.85	0.985
0.50	5.80	0.0987
1.00	8.44	0.988
	47.3 (λ_2)	0.010 (C_2')
2.00	12.67	0.993
3.00	16.91	0.995
5.00	25.19	0.997
10.00	48.50	0.998
20.00	85.70	0.999

An alternative approach to solving the set of differential equations is to employ Runge-Kutta integration. This approach was rewarding as the problem could be collapsed so only one initial condition (for the integration leading to γ) was required. In addition, a reformulation of eq. 8 led to an expression whose asymptotic behavior at large B could be extracted. The matrix and Runge-Kutta results agreed where both could be used.

Using $n' = 1$ as an example (the asymptotic form may be found easily for arbitrary n') we write

$$\gamma = c\int_{-1}^{1} \mathrm{d}x x G(x, t) \tag{11}$$

where

$$G(x, t) = \int_{-1}^{1} \mathrm{d}x' x' \exp(-BV(x'))\, P(x, x', t). \tag{12}$$

It is easy to show that

$$\frac{\partial G}{\partial t} = \frac{\partial^2 G}{\partial x^2} + B\left(\frac{\partial V}{\partial x}\frac{\partial G}{\partial x} + G\frac{\partial^2 V}{\partial x^2}\right) \tag{13}$$

i.e., G obeys the same differential as P.

The initial condition is (from eq. 12)

$$G(x, 0) = x \exp(-BV(x)) \tag{14}$$

Thus, if $G(x, t)$ is determined (by Runge-Kutta integration here) $\gamma(t)$ may be found and fit to a sum of exponentials (eq. 10) to extract the decay rates and corresponding amplitudes. The results of this approach (model A) are shown for $n' = 1$ and $B = 1$ in table 2.

Results for $n' = 2$ are shown in table 3. Again, the dominance of λ_1 is seen, the effect becoming more pronounced as B increases. In addition, one sees that λ_1 increases with B.

The upturn in λ_1 for small B is an artifact of the numerical method related to the effective boundary conditions imposed by the conversion of the differential equation to difference equations. For large B the results correspond to the (desired) boundary condition $\partial P/\partial z = 0$ at the end points. For small B the boundary condition for the numerical results is $P = 0$. Thus, to obtain values for the boundary condition $\partial P/\partial z = 0$ and small B, one must extrapolate from the large B results.

Table 3

First relaxation mode parameters ($n' = 2$)

B	c_1'	λ_1	Grid size	c_1'	λ_1	Grid size
0.0278	0.785	15.1	101	0.595	19.5	51
0.100	0.952	11.6	111	0.671	19.8	51
0.250	0.985	8.84	101	0.952	9.42	51
0.500	0.991	8.43	111	0.959	11.9	51
1.00	0.987	12.6	111	0.980	14.3	51
3.00	0.989	29.5	101	0.974	30.4	51
5.00	0.994	46.6	91	0.990	48.0	51
7.50	0.993	67.7	111	0.993	68.9	51
12.5	0.996	110.0	111	0.992	118.0	51
17.5	0.996	152.0	101	0.991	170.0	51

The effect of grid size is also seen in the data. λ_1 is reasonable converged for $1 < B < 5$. The results are still grid size dependent for small (especially) and large B.

For $n' = 1$ the problem was avoided by employing a variable grid spacing near the end points.

A detailed discussion of these numerical effects appears in ref. 4.

It is useful to consider the asymptotic form of eq. 13 for large B. For the one-dimensional case we presume

$$G = g(x)\exp(-\lambda t) \tag{15}$$

Table 4

Upper and lower bounds for the dominant rate ($L = 51$ nm) (upper bounds for $n' = 50$ and $n' = 100$ estimated using fig. 5)

n'	Upper bound	Lower bound
1	3.407	0.112
3	3.634	0.377
4	4.115	0.532
5	4.363	0.698
6	4.615	0.875
8	5.148	1.25
9	5.4	1.45
10	5.7	1.66
15	7.2	–
20	8.7	4.0
25	9.8	–
30	10.4	6.7
50	17.3	12.6
100	34.7	29.4

Inserting eq. 15 into eq. 13 yields

$$-\lambda g = \frac{\partial^2 g}{\partial x^2} + B\left(\frac{\partial V}{\partial x}\frac{\partial g}{\partial x} + g\frac{\partial^2 V}{\partial x^2}\right). \tag{16}$$

Since eq. 14 is a known solution we may insert it into eq. 16 and find

$$\lambda/B = (\partial V/\partial x)/x \tag{17}$$

By considering the asymptotic limit we have swamped out the contribution of free diffusion. Free diffusion is expected to enhance the relaxation rate. Thus, the λ in eq. 17 may be considered to be a lower bound to λ_1 for any B. This is proved in appendix B. Upper bounds on λ_1 are found in appendix A.

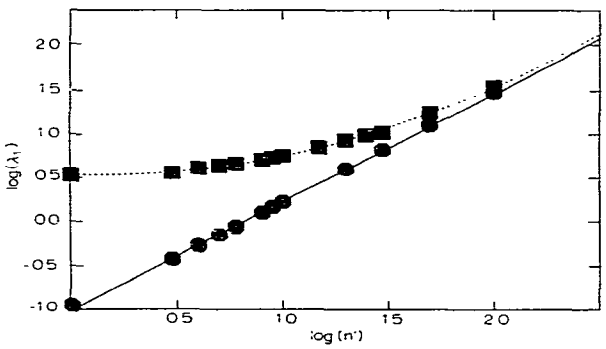

Fig. 5. Bounds for the slowest rate. (Circles) Lower bound. (Squares) Upper bound. (Solid line) Linear fit. (Dotted line) Quadratic fit.

The values of the bounds on λ_1 for $B = 0.028$ and $L = 51$ nm (our model case) as a function of n' are shown in table 4 and plotted in fig. 5. For large n' the bounds are coalescing and we estimate $\lambda_1 = 83$ for $n' = 228$ (the Manning condensation theory estimate for n' for our DNA fragment [7]). Note that the (dominant) relaxation rate increases with n' in contrast to the conclusion reached in previous work [1].

4. Conclusions

The magnitude of the dielectric increment as reflected in the amplitude of the dipolar correlation function is computed for a model linear array as a function of the number of counterions and the lengths of the (model) polyelectrolyte. As the number of counterions increases the correlation function amplitude rises rapidly to a maximum and then decreases slowly.

The most probable configuration of counterions is computed and found to be a double helix with a pitch corresponding to that of the phosphate backbone of DNA for cylinder dimensions and number of counterions corresponding to that of a typical DNA fragment. This result suggests that electrostatic interactions may play a significant role in determining the structure of DNA.

The counterion repulsions are found to play a major role in the dynamics. Longitudinal diffusion under the influence of the potential of the counterions leads to a correlation function which is essentially a single exponential with a rate constant which increases with increasing interaction between counterions. This finding is opposite to a supposition made in our previous work. Upper and lower bounds for the relaxation rate are found. These bounds approach each other when parameters typical of DNA are assigned. Depending on the magnitude of the one-dimensional diffusion constant (estimate $D_1 = 10^{-11}$ m^2 s^{-1}) the dielectric dispersion of a 51 nm segment of DNA (due to the longitudinal motion of the counterions) would occur in the vicinity of 1 MHz where it would partly overlap the 'high frequency' dispersion which we assigned previously [2] to transverse diffusion on the polyelectrolyte surface. Longer DNA samples would absorb at lower frequencies.

5. Response to reviewers comments

Interesting comments and analyses were received from a referee. We reply below.

5.1. Screening

In refs. 1 and 2, Debye screening was included in eq. 4. This softens the potential and increases $\lambda(0)$, particularly for large n'. However, inclusion of screening is inconsistent with the two-phase (condensed-free) picture for the counterions. The model (the physical reasonableness of which is certainly open to discussion) treats the condensed counterions explicitly. No additional counterions are available in the condensed phase for screening and the concentration of coions is negligibly small.

Certainly, screening (or introduction of a 'convergence factor' in the spirit of Mayer's theory of ionic solutions) would facilitate solution of eq. 8 via Fourier transformation as pointed out by the reviewer. This appears to be an avenue worth pursuing.

5.2. Other potentials

The reviewer suggested examining the nature of the minimum-energy configuration using

$$V/k_B T = \sum_{j<i} \sum_{i} Q^2/(z_i - z_j)^2 \tag{18}$$

with

$$Q = e^2/4\pi\epsilon\epsilon_0 k_B T \tag{19}$$

in place of eq. 4.

This potential is qualitatively similar to eq. 4, having softer interactions with distant neighbors. Varying the form of the potential as well as the values of n' and B would provide a broader picture of the role of electrostatic interactions in inducing the double-helix configuration. Of particular interest is the dependence of the helix spacing on the potential and parameters chosen.

5.3. Phase transitions

If configurational phase space is restricted (by increasing B with n' fixed or for large n'), one expects $\lambda(0)$ to decrease.

For a three-dimensional system solidification (with $\gamma(0) = 0$) occurs if the mean square displacement of the particles from their minimum-energy configuration becomes less than a critical value which depends on the nature of the potential. For the inverse first-power potential employed here the empirical Lindemann criterion may be used [10]. As calculated by the referee the Lindemann criterion predicts a phase transition for $(n'B)^{-1} \lesssim 0.02$. Some of the entries in table 1 are approaching this limit.

The idea is that incipient solidification is responsible for stopping the growth of $\gamma(0)$. In fact, the freedom of motion in the radial direction is greater than that described in the longitudinal direction (by the model calculation). Thus, the actual $\gamma(0)$ may not show the behavior of the one-dimensional model calculation.

Of course a one dimensional system does not show a phase transition [11] so the Lindemann criterion cannot be applied strictly to the model calculation. On the other hand, the model calculation is set forth as providing proper qualitative predictions for the real (three-dimensional) system.

The only had evidence that the observed behavior of $\gamma(0)$ is representative of the mobile phase is that similar behavior for the longitudinal component was found in ref. 2 where the integrals were taken over the transverse as well as the longitudinal coordinate (a two-dimensional system). To maintain the two-phase picture in a three-dimensional system the counterions could be allowed to move in an appropriately chosen cylindrical shell surrounding the polyion.

Appendix A

A1. Sum rules and upper bounds

Our master equation, eq. 8, is a special case of the general form [8]

$$\partial P/\partial t = \hat{O}P \tag{A1}$$

where $\hat{O}$ is a time-independent operator in the configuration coordinate set $\{x_i\}$ and P a function of $\{x_i\}$, $\{x_i'\}$ and t. The primed coordinates specify the system configuration at $t = 0$. The distribution of the primed coordinates is given by

$$P_{eq} = c \exp(-BV(\{x_i'\})) \tag{A2}$$

where V is the energy in scaled units and c a normalization constant.

The space and time variables are separable in eq. A1 with the result

$$P(t) = \sum_j P_j(\{x_i\}, \{x_i'\}) \exp(-\lambda_j t) \tag{A3}$$

Averages over $P(t)$ and P_{eq} (such as γ) such appear as sums of exponentials. Such an average is the correlation function

$$\begin{aligned}\langle f_1(0) \cdot f_2(t) \rangle &= c \int\int \prod_i dx_i' f_1(\{x_i'\}) \exp(-BV(\{x_i'\})) \\ &\quad \cdot \int\int \prod_i dx_i f_2(\{x_i\}) P(\{x_i\}, \{x_i'\}, t) \\ &= \sum_j c_j \exp(-\lambda_j t)\end{aligned} \tag{A4}$$

Clearly

$$P(0) = \prod_i \delta(x_i - x_i') \tag{A5}$$

Differentiating eq. A4 with respect to time N times and evaluating the result as t approaches zero yields

$$C^N(0) = \lim_{t \to 0} \frac{\partial^N}{\partial t^N} \langle f_1(0) \cdot f_2(t) \rangle = (-1)^N \sum_j c_j \lambda_j^N \tag{A6}$$

However, $C^N(0)$ may be evaluated by a separate route using the operator identity

$$\lim_{t \to 0} \frac{\partial^N}{\partial t^N} = \lim_{t \to 0} \hat{O}^N \tag{A7}$$

which applied to P yields

$$\lim_{t \to 0} \frac{\partial^N P}{\partial t^N} = \hat{O}^N \prod_i \delta(x_i - x_i') \tag{A8}$$

since $\hat{O}$ is independent of t.

Changing the order of integration in eq. A4 and integrating over $\{x_i'\}$ yields (applying the operator of eq. A8)

$$\begin{aligned}C^N(0) = c \int\int \prod_i dx_i f_2(\{x_i\}) \hat{O}^N \int\int \prod_i dx_i' f_1(\{x_i'\}) \\ \cdot \exp(-BV(\{x_i'\})) \prod \delta(x_i - x_i')\end{aligned}$$

$$= c\int\int\prod_i \mathrm{d}x_i f_2(\{x_i\}) \times \hat{O}^N[f_1(\{x_i\})\exp(-BV(\{x_i\}))] \quad \text{(A9)}$$

For γ we set

$$f_1 = f_1 = \sum x_i \quad \text{(A10)}$$

and (in scaled time units)

$$\hat{O} = \sum \frac{\partial}{\partial x_i}\exp(-BV)\frac{\partial}{\partial x_i}\exp(BV) \quad \text{(A11)}$$

Evaluation of the multiple integral (quotient) of eq. A9 yields $C^N(0) \equiv \gamma^N(0)$.

These integrals become difficult as n' becomes large and the task is similar to the evaluation of $\gamma(0)$ itself.

Thus, the evaluation of a set $C^N(0)$ and inversion to find a (truncated) collection $\{c_i, \lambda_i\}$, thereby bypassing the solution of the full equation for the dynamics, is not practicable for moderate to large n'.

Explicit expressions for the first four sum rules were found [4]. The first two are of most interest.

$$\sum c_i = \gamma(0) \quad \text{(A12)}$$

$$\sum c_i\lambda_i = n' \quad \text{(A13)}$$

The convergence of the sums in eqs. A12, A13 and higher sum rules was tested [4] using results of solving the dynamics for small n'. Both the extraction of the $\{c_i, \lambda_i\}$ from the sum rules and the verification of the sum rules by evaluation of the sums from the dynamical results were in accord with the quality of the data base. These calculations confirm the correctness of the manipulation of the delta functions leading to eq. A9.

Our interest in the sum rules eqs. A12 and A13 is to derive upper bounds for λ_1 (the smallest λ_i).

Multiplying eq. A12 by λ_1 and subtracting the result from eq. A13 gives

$$\lambda_i + \sum_{i=2}^{\infty} c_i(\lambda_i - \lambda_1)/\gamma(0) = n'/\lambda(0) \quad \text{(A14)}$$

Since C_i, $\gamma(0) > 0$ and $\lambda_i > \lambda_1$ we derive the bound

$$n'/\gamma(0) > \lambda_1 \quad \text{(A15)}$$

Values of $n'/\gamma(0)$ are shown in table 2 ($L = 51$ nm).

Appendix B

B1. The Langevin equation and lower bounds

If the Langevin equation [9] were chosen to describe the dynamics of our model system, the equations of change would have the form

$$m\ddot{x}_i + k_B T\dot{x}_i/D_1 = -(2/L)^2 Bk_B T\frac{\partial V(\{x_i\})}{\partial x_i} + R_i(t) \quad \text{(B1)}$$

where m is the mass of an ion and $R_i(t)$ the random force acting on the i-th ion at time t.

It is instructive to solve the set of equations (eq. B1) with $m = R_i(t) = 0$. In this limit the coordinates evolve in a deterministic fashion from the original configuration to the configuration of minimum energy. The potential surface for our system appears to be such that evolution to local minima does not occur. The equations of change may be solved by (fourth order) Runge-Kutta integration and the method is convenient for finding the configuration of lowest energy. Fig. 1 shows the result of an application to cylindrical geometry.

The deterministic description of the system dynamics is related to the large B limit of the stochastic description of eq. 8.

For the linear model the system dipole moment is

$$\mu = \sum_{i=1}^{n'} x_i \quad \text{(B2)}$$

For $\{x_i\}$ sufficiently close to the configuration of minimum energy only the term with the slowest rate will contribute to the decay of μ

$$\mu = \alpha\exp(-\tilde{\lambda}t) \quad \text{(B3)}$$

so that

$$\dot{\mu} = -\tilde{\lambda}\alpha\exp(-\tilde{\lambda}t) \quad \text{(B4)}$$

and $\tilde{\lambda}$ is the deterministic analog of λ_1 ($\tilde{\lambda}$ has units of $4D_1/BL^2$).

Combining eqs. B1–B4 yields

$$\tilde{\lambda} = \sum_i \frac{\partial V}{\partial x_i}/\sum_i x_i \quad \text{(B5)}$$

where the sums are evaluated for $\{x_i\}$ approach-

ing the minimum-energy configuration along a deterministic trajector.

Comparing eq. B5 with the asymptotic form (large B) from the stochastic description we find

$$\lambda_1/B > \lim_{B\to\infty}(\lambda_1/B) = \sum_i \frac{\partial V}{\partial x_i} \Big/ \sum_i x_i = \tilde{\lambda} \qquad \text{(B6)}$$

Thus, $\tilde{\lambda}B$ provides a lower bound to λ_1.

Values of $\tilde{\lambda}B$ ($L = 51$ nm) are shown in table 2.

Acknowledgement

This work was supported by a National Institutes of Health Grant GM-0425.

References

1 P.I. Meyer and W.E. Vaughan, Biophys. Chem. 12 (1980) 329.
2 P.I. Meyer, G.E. Wesenberg and W.E. Vaughan, Biophys. Chem. 13 (1981) 265.
3 R.J. Gillespie, Can. J. Chem. 38 (1960) 818.
4 G.E. Wesenberg, Thesis, University of Wisconsin-Madison (1983).
5 W.E. Vaughan, Adv. Mol. Relax. Inter. Proc. (J. Mol. Liq.) 22 (1982) 121.
6 B. Carnahan, H.A. Luther and J.O. Wilkes, Applied numerical analysis (John Wiley and Sons, New York, 1969).
7 G.S. Manning, J. Chem. Phys. 51 (1969) 924.
8 I. Oppenheim, K.E. Shuler and G.H. Weiss, Stochastic processes in chemical physics: The master equation (MIT Press, Cambridge, 1977).
9 S.W. Lovesey, Condensed matter physics: Dynamic correlations (Benjamin/Cummings, London, 1980).
10 J.P. Hansen and I.R. McDonald, Theory of simple liquids (Academic Press, London, 1976) section 10.6.
11 I.Z. Fisher, Statistical theory of liquids (University of Chicago Press, Chicago, 1964) ch. 1.